Bindi, D., Gomez Capera, A. A., Parolai, S., Abdrakhmatov, K., Stucchi, M., Zschau, J. (2013): Location and magnitudes of earthquakes in Central Asia for seismic intensity data: model calibration and validation. - Geophysical Journal International, 192, 2, pp. 710—724.

DOI: http://doi.org/10.1093/gji/ggs039

Geophysical Journal International

Geophys. J. Int. (2013) **192,** 710–724 doi: 10.1093/gji/ggs039

Location and magnitudes of earthquakes in Central Asia from seismic intensity data: model calibration and validation

Dino Bindi,[1] Augusto A. Gómez Capera,[2] Stefano Parolai,[1] Kanatbek Abdrakhmatov,[3] Massimiliano Stucchi[2] and Jochen Zschau[1]

[1] *Deutsches GeoForschungsZentrum GFZ, Section* 2.1, *Telegrafenberg,* 14473 *Potsdam, Germany. E-mail: bindi@gfz-potsdam.de*
[2] *Istituto Nazionale di Geofisica e Vulcanologia, via Bassini* 15, 20133 *Milano, Italy*
[3] *Institute of Seismology, National Academy of Science, Bishkek, Kyrgyz Republic*

Accepted 2012 October 22. Received 2012 October 22; in original form 2012 June 19

SUMMARY

In this study, we estimate the location and magnitude of Central Asian earthquake from macroseismic intensity data. A set of 2373 intensity observations from 15 earthquakes is analysed to calibrate non-parametric models for the source and attenuation with distance, the distance being computed from the instrumental epicentres located according to the International Seismological Centre (ISC) catalogue. In a second step, the non-parametric source model is regressed against different magnitude values (e.g. M_{LH}, m_b, M_S, M_w) as listed in various instrumental catalogues. The reliability of the calibrated model is then assessed by applying the methodology to macroseismic intensity data from 29 validation earthquakes for which both M_{LH} and m_b are available from the Central Asian Seismic Risk Initiative (CASRI) project and the ISC catalogue. An overall agreement is found for both the location and magnitude of these events, with the distribution of the differences between instrumental and intensity-based magnitudes having almost a zero mean, and standard deviations equal to 0.30 and 0.44 for m_b and M_{LH}, respectively. The largest discrepancies are observed for the location of the 1985, $M_{LH} = 7.0$ southern Xinjiang earthquake, whose location is outside the area covered by the intensity assignments, and for the magnitude of the 1974, $m_b = 6.2$ Markansu earthquake, which shows a difference in magnitude greater than one unit in terms of M_{LH}. Finally, the relationships calibrated for the non-parametric source model are applied to assign different magnitude-scale values to earthquakes that lack instrumental information. In particular, an intensity-based moment magnitude is assigned to all of the validation earthquakes.

Key words: Seismicity and tectonics; Seismic attenuation; Asia.

INTRODUCTION

Macroseismic intensities are widely used in many seismological applications, ranging from studies on the source properties of earthquakes that occurred in the pre-instrumental period to the generation of maps providing a rapid description of the post-earthquake spatial distribution of damage. Moreover, in many region of the world where there is inadequate coverage by strong motion instrumentation to allow the calibration of reliable local ground motion prediction equations (e.g. in Central Asia), intensity values are a fundamental ingredient for assessing the seismic hazard. When historical and instrumental catalogues are merged, compatibility issues regarding the source parameters (i.e. magnitude and locations) can arise. To this regard, several methods have been proposed to relate intensity to epicentral parameters (e.g. Evernden 1975; Hanks *et al.* 1975; Toppozada 1975; Evernden *et al.* 1981; Toppozada *et al.* 1981; Gasperini *et al.* 1999; Toppozada & Branum 2002; Gasperini *et al.* 2010; Bakun *et al.* 2011). In particular, Bakun & Wentworth (1997, 1999) introduced an approach to determine both the location and magnitude of earthquakes directly from intensity. The methodology is calibrated by considering a set of earthquakes for which both instrumental epicentral parameters and intensity values are available. The calibration step aims at developing an attenuation relationship that describes the decay of intensity with distance from the instrumental epicentre and describing the earthquake's size according to an instrumental magnitude scale. Then, in applying the method, the intensity epicentre and the corresponding intensity magnitude are determined through a grid search procedure over a grid of trial epicentres, computing the single station magnitudes by applying the calibrated intensity attenuation, and minimizing the root mean square residual between single station magnitude and their average. The method has been applied to several data sets (e.g. see Mezcua *et al.* 2004; Beauval *et al.* 2010; Choy *et al.* 2010; Alvarez-Rubio *et al.* 2011; Bakun *et al.* 2011 and the reference cited therein)

confirming its suitability to estimate location and magnitude from intensity, as well as to assigning an uncertainty to each estimate.

In this study, we apply a modified version of the methodology proposed by Bakun & Wentworth (1997) to a set of earthquakes that occurred in Central Asia. In particular, we calibrate a non-parametric model for describing the dependence of intensity on distance and earthquake size, without explicitly involving any magnitude scale in the calibration. The non-parametric source coefficients are afterwards regressed against any known description of a source's size (e.g. values associated with for different magnitude scales). Finally, the model is validated using a set of independent earthquakes included in the ISC catalogue.

DATA

We analyse 44 earthquakes that occurred in Central Asia over the time period 1965–1992 (Fig. 1). For each earthquake, the distribution of the macroseismic intensities, in terms of the MSK-64 scale (Medvedev *et al.* 1964), has been retrieved as one of the outcomes of the Central Asian Seismic Risk Initiative (CASRI) project and are also listed in Januzakov *et al.* (2003). A detailed description about the methods and procedures applied to analyse intensity data in the former Soviet Union can be found in Kondorskaya & Shebalin (1982).

Tables 1 and 2 present the main epicentral parameters of the earthquakes of interest as provided by several international agencies. In the CASRI catalogue, the magnitude is measured according to the Moscow-Prague formula (Karnik 1962), and it is generally indicated as M_{LH} in the Russian scientific literature. For a thorough discussion on the definition of this magnitude scale and its relationship to the surface wave magnitude introduced by Gutenberg (1945), we refer the reader to Bormann (2002) and the references cited therein. In the former Soviet Union, the size of earthquakes recorded by local and regional networks was routinely quantified by computing the energy-class K (Rautian 1960; Rautian *et al.* 2007), which is based on the sum of the maximum amplitudes of *P* and *S* waves. The energy-class K for the earthquakes considered in this study ranges from 12 to 17.

The other information listed in Tables 1 and 2 are the locations and magnitudes from the ISC bulletin (International Seismological Centre, http://www.isc.ac.uk/) and from the Global Centroid Moment Tensor catalogue (GCMT catalogue, http://www.globalcmt.org). Regarding the ISC parameters, the EHB solutions (Engdahl *et al.* 1998) are considered. Fig. 2 shows the differences between the CASRI and ISC hypocentral location estimates, with the horizontal distances between the estimates being less than 20 km, with about 70 per cent of the differences being less than 10 km. The depths provided by ISC vary between 2.5 and 46 km, with a mean depth of about 20 km, whereas the depths in the CASRI catalogue span the range from 5 to 30 km. The lack of any clear correlation between the depths reported in the different catalogues (see Fig. 2) indicates that this parameter is poorly constrained in at least one of the considered catalogue. In any case, focal depth is not expected to play a critical role in the analysis performed in this study (Bakun, personal communication).

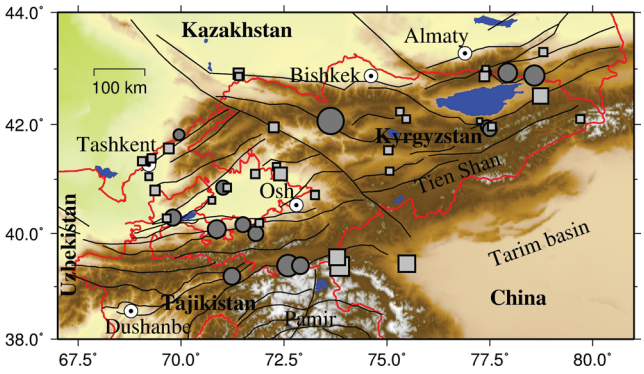

Figure 1. Map of the study area showing the main active faults (black lines). Epicentres of earthquake used to calibrate the method are shown as dark grey filled circles (Table 1), whereas those used for validation are shown as light grey filled squares (Table 2). The size of the symbols is proportional to the earthquake's magnitude.

The considered earthquake catalogue is divided into two subsets. The first is used to calibrate an attenuation model (calibration data set, Table 1) whereas the second (validation data set, Table 2) is used to validate the inferred model by considering data independent from those used to calibrate the model. The calibration data set contains earthquakes that occurred after 1976 and are included in the GMCT and ISC catalogues (Fig. 3, left), whereas the validation data set includes earthquakes that occurred between 1964 and 1976 and are listed in the ISC catalogue (Fig. 3, right). Fig. 3 also shows the location of the earthquakes (top panels), as well as the intensity versus distance distributions (middle).

In the validation data set, we also include the 1985 August 23 southern Xinjiang (China) earthquake (red circles in Fig. 3) and the 1974 August 11 Markansu earthquake (green circles). Although these earthquakes are not good candidates as validation earthquakes since they occurred at the border of the investigated region and are characterized by an incomplete macroseismic field, the analyses of these two special cases can provide useful hints for discussions when the models derived in this study are applied to historical earthquakes in that region. As an example, Fig. 4 shows the intensity distributions for two earthquakes, namely earthquake ID 54 (Table 1), corresponding to the earthquake with the largest number of available intensity values (359), and earthquake ID 63 (Table 2) corresponding to the earthquake with the lowest number of available intensity values (25).

TECTONIC SETTINGS

The investigated area is centred on the Pamir and Tien Shan mountain belts and is bordered by two stable crustal elements, the Tarim basin to the southwest and the Kazakh platform to the north. The Pamirs and Tien Shan are two of the major Cenozoic mountain belts in Central Asia. They are the result of the India-Eurasia collision, with the Indian Plate migrating northwards during the Cretaceous and Palaeogene at a rate of 15–20 cm/yr, slowing down to its present rate of approximately 5 cm yr^{-1} following its initial collision during Eocene (Patriat & Achache 1984). A significant proportion of this post-collisional lithospheric convergence is accommodated by the convergence of Pamir and Tien Shan. The Tien Shan can be considered as a prototypical active intracontinental mountain belt, where widespread deformation occurs on reverse faults and intramountain basins that are far from the boundaries of the major plates (Zubovich *et al.* 2010). The Pamir has been displaced northwards by about 600 km with respect to the Tarim Basin (Burtman & Molnar 1993) and it is characterized by east–west trending thrust faults and major strike-slip faults flanking the range (Lukk *et al.* 1995). Recent studies (e.g. Zubovich *et al.* 2010) showed that most of the convergence between the Tarim Basin and the Kazakh platform is absorbed within the Tien Shan, presumably by slip on thrust or reverse faults. The convergence between the Tarim basin and the Kazakh platform

Table 1. Locations and magnitudes of the earthquakes making up the calibration data set as reported by different catalogues (CASRI, ISC, GCMT). Npt is the number of available intensity values; D is the depth in kilometres; I_{min} and I_{max} represent the minimum and maximum intensity values, respectively.

ID	Date	Npt	$I_{min}-I_{max}$	CASRI					ISC					GCMT				
				Lat	Lon	D	M_{LH}	K	Lat	Lon	D	M_S	m_b	Lat	Lon	D	M_S	M_w
54	1/31/1977	359	2.5–7.5	40.08	70.87	20	6.3	15.5	40.082	70.861	35	–	6.0	39.85	69.79	10	5.9	6.0
55	6/3/1977	135	2.0–6.5	40.00	71.82	15	5.8	14.2	39.945	71.839	14	–	5.0	39.62	70.92	24	5.0	5.3
21	3/24/1978	290	2.5–8.0	42.88	78.58	22	6.6	15.6	42.833	78.568	23.8	7.2	6.1	42.37	78.69	34.7	7.1	6.9
72	11/1/1978	216	2.0–8.0	39.40	72.60	30	6.8	16.2	39.362	72.587	23.3	6.8	5.9	39.34	72.16	15	6.8	6.6
22	4/6/1979	48	2.0–5.5	41.97	77.43	25	5.3	13.5	41.877	77.597	11.5	5.2	5.1	41.92	77.74	19	4.9	5.3
23	7/5/1980	34	3.5–6.0	41.92	77.50	20	5.6	13.8	41.876	77.424	11.4	5.3	5.4	41.94	77.40	15	5.2	5.4
58	5/6/1982	206	2.0–7.5	40.17	71.50	20	5.8	14.4	40.145	71.533	30.2	5.7	5.5	40.26	71.42	15	5.6	5.7
73	12/16/1983	57	2.5–7.0	39.40	72.90	15	6.1	14.6	39.356	72.941	9.4	5.9	5.7	39.32	72.48	15	5.6	5.9
59	2/17/1984	67	3.0–8.0	40.85	71.02	10	5.6	14.1	40.852	71.083	14.8	5.4	5.4	41.13	70.84	12	5.2	5.5
74	10/26/1984	148	2.0–7.5	39.20	71.23	15	6.1	14.8	39.164	71.347	9	6.2	5.9	38.99	71.03	12	6.1	6.1
61	10/13/1985	313	2.0–8.0	40.30	69.80	10	6.0	14.8	40.336	69.812	16	6.0	5.8	40.22	69.20	10	5.9	5.8
62	3/26/1987	153	2.0–6.5	41.82	69.95	5	5.0	13.1	41.788	69.875	18.2	4.6	5.1	42.44	70.02	15	4.5	5.2
28	6/17/1988	38	3.0–6.0	42.93	77.40	21	4.9	12.9	42.950	77.511	17.3	5.4	5.2	43.01	77.51	15	5.3	5.6
29	11/12/1990	208	3.0–8.0	42.93	77.93	15	6.4	15.3	42.955	78.056	19	6.3	5.8	43.18	78.24	15	6.3	6.3
30	8/19/1992	101	4.5–9.5	42.07	73.63	25	7.3	17.0	42.106	73.603	27	7.3	6.5	42.19	73.32	17	7.4	7.2

Table 2. Locations and magnitudes of the earthquakes making up the validation data set as reported by the CASRI and ISC catalogues. Npt is the number of available intensity values; D is the depth in kilometres; I_{min} and I_{max} represent the minimum and maximum intensity values, respectively.

ID	Date	Npt	$I_{min}-I_{max}$	CASRI					ISC				
				Lat	Lon	D	M_{LH}	K	Lat	Lon	D	M_S	m_b
45	3/17/1965	78	3.0–7.0	40.80	69.37	12	5.5	13	40.838	69.33	35	–	5
12	9/25/1965	95	3.0–6.0	41.53	75.03	25	5.2	13	41.509	75.017	16.8	–	5.2
13	10/18/1965	37	2.5–6.0	41.97	77.55	15	5	13	41.972	77.509	35	–	5.2
46	4/25/1966	151	3.0–6.0	41.38	69.28	8	5.1	13.3	41.327	69.151	3.1	–	4.8
47	4/30/1966	71	3.0–6.5	41.10	71.80	20	5.2	13.6	41.083	71.945	20.9	–	4.9
48	5/18/1967	70	3.0–6.5	40.62	70.75	25	4.6	12	40.663	70.569	35	–	4.6
14	9/28/1967	33	3.0–6.0	42.10	79.70	18	5.1	13.5	42.148	79.648	19.1	–	4.8
15	11/30/1967	45	3.0–6.0	43.00	77.40	10	4.5	12	–	–	–	–	–
16	3/20/1968	29	2.0–5.5	41.15	75.07	17	4.9	12.6	41.034	75.191	10	–	4.7
49	1/19/1970	59	3.0–7.0	41.05	69.22	25	4.7	12.1	41.2	69.212	20.2	–	4.8
17	6/5/1970	109	3.0–7.0	42.52	78.73	15	6.8	15.6	42.498	78.724	3.1	–	5.9
18	5/10/1971	39	3.0–6.5	42.92	71.40	20	5.7	14	42.838	71.318	15.7	–	5.6
50	10/28/1971	88	3.0–6.0	41.95	72.25	17	5.6	14	41.854	72.332	38.3	–	5.4
51	3/17/1972	148	3.0–6.5	40.28	69.65	20	5	13.5	40.1	69.681	26.3	–	5.1
52	1/22/1974	52	3.0–7.0	40.20	71.90	24	5	12.7	40.119	71.799	35	–	4.6
53	2/20/1974	74	3.0–6.5	40.72	73.25	15	5.1	13.2	40.674	73.243	26.8	–	4.8
19	7/2/1974	39	3.0–6.5	42.23	75.32	15	4.9	12.9	42.297	75.399	12.2	–	4.6
71	8/11/1974	69	2.0–6.5	39.38	73.85	15	7.3	16.6	39.372	73.797	5	–	6.2
20	2/12/1975	62	2.5–6.0	43.30	78.80	10	5.1	13	43.156	78.943	4.7	–	5.3
56	12/6/1977	69	2.0–6.5	41.57	69.70	15	5.6	14	41.56	69.689	16.7	–	5.2
57	12/11/1980	160	2.5–7.0	41.33	69.05	10	5.1	13.5	41.327	69.104	10.9	4.8	5
24	12/31/1982	139	2.5–6.0	42.87	77.37	15	5.6	13.6	42.796	77.423	24	5.1	5.8
25	12/21/1983	43	2.5–6.0	42.07	77.25	20	4.1	12.5	42.077	77.471	15	–	4.8
26	2/2/1984	53	2.5–6.0	42.87	71.40	15	4.8	12.6	42.939	71.361	24.7	–	5.2
60	4/27/1985	79	2.0–7.5	40.85	71.12	15	4.9	12.8	40.89	71.159	13.8	4.4	5.1
27	3/13/1988	40	3.0–6.0	42.10	75.47	7	4.9	12.6	42.131	75.362	15	–	4.4
63	12/21/1988	25	2.5–6.0	41.23	72.32	10	4.8	12.9	41.175	72.32	45.9	4.7	5.4
64	5/15/1992	36	4.0–8.0	41.10	72.42	10	6.3	15.3	40.998	72.47	35.7	6.2	5.6
75	8/23/1985	102	2.0–7.0	39.43	75.48	20	7	16.5	39.45	75.25	2.5	7.3	6.2
90	5/10/2008	37	3.0–8.0	39.53	73.75	29	6.9	15.4	39.558	73.791	29	6.9	6.2

is absorbed over a region more than 200-km wide and although not uniformly distributed, no single predominant fault absorbs the majority of this convergence. The Pamir seems to move northward towards Eurasia with its northern part diverging westwards from the Tarim Basin at 5–8 mm yr^{-1} (Zubovich *et al.* 2010).

In the last two centuries, several strong earthquakes occurred in central Asia (e.g. Kondorskaya & Shebalin 1982). Examples are the strong earthquakes that struck the northern Tien-Shan between the end of the XIX and the beginning of the XX century ($M = 7.3$, 1887 Verny earthquake; $M = 8.2$, 1889 Chilik earthquake; $M = 8.2$, 1911 Kemin earthquake; $M = 6.9$, 1938 Chu-Kemin earthquake). The occurrence of such large earthquakes makes Central Asia one of the areas of the world most prone to earthquake hazard, as confirmed by several studies performed at different spatial scales (e.g. Ulomov 1999; Abdrakhmatov *et al.* 2003; Erdik *et al.* 2005; Bindi *et al.* 2012). Since most of these studies are based on seismic

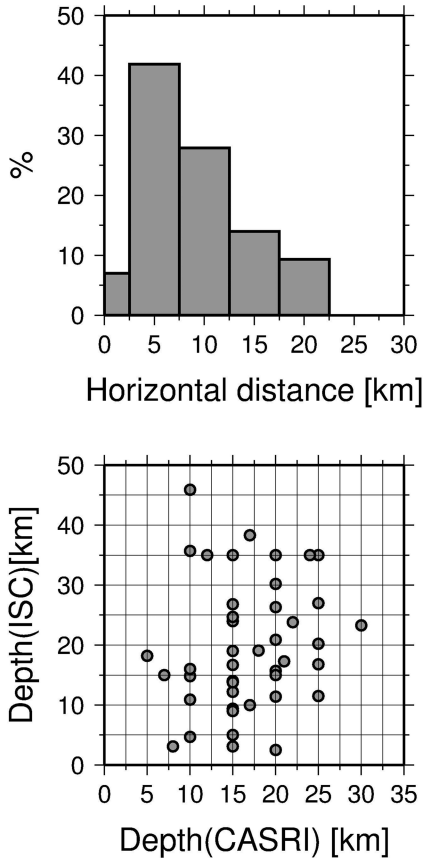

Figure 2. Comparison between the locations listed in the ISC and CASRI catalogues. Top panel: histograms of horizontal distances between the epicentre estimates; bottom panel: ISC versus CASRI depths (see Tables 1 and 2).

catalogues including both historical and instrumental earthquakes, in this paper we follow the approach of Bakun & Wentworth (1997) to calibrate, using instrumental data, a model for estimating magnitude and location of earthquakes form intensity data.

METHODOLOGY

Bakun & Wentworth (1997) approach

In their paper, Bakun & Wentworth (1997) proposed a method (hereinafter referred to as BW97) to estimate the magnitude and location of historical earthquakes directly from intensity estimates. The method develops in two main steps.

In the first step, the intensities for earthquakes with well-constrained magnitudes and locations (i.e. the calibration data set) are used to calibrate a parametric model describing the intensity values as a function of magnitude and distance. A typical model is expressed as

$$I_{ij} = c_0 + c_1 M_j + c_2 \log_{10}(\Delta_{ij}) + c_3 \Delta_{ij}, \quad (1)$$

where M_j is the magnitude of the jth earthquake (with $j = 1,\ldots,$ N_{eq}, where N_{eq} the number of considered earthquake), Δ_{ij} is the hypocentral distance for earthquake j recorded at site i and I_{ij} is the relevant intensity value. The model parameters (c_0, c_1, c_2 and c_3) are generally determined through a least-square regression, either in one step (e.g. Bakun & Wentworth 1997) or in two steps (Bakun & Scotti 2006).

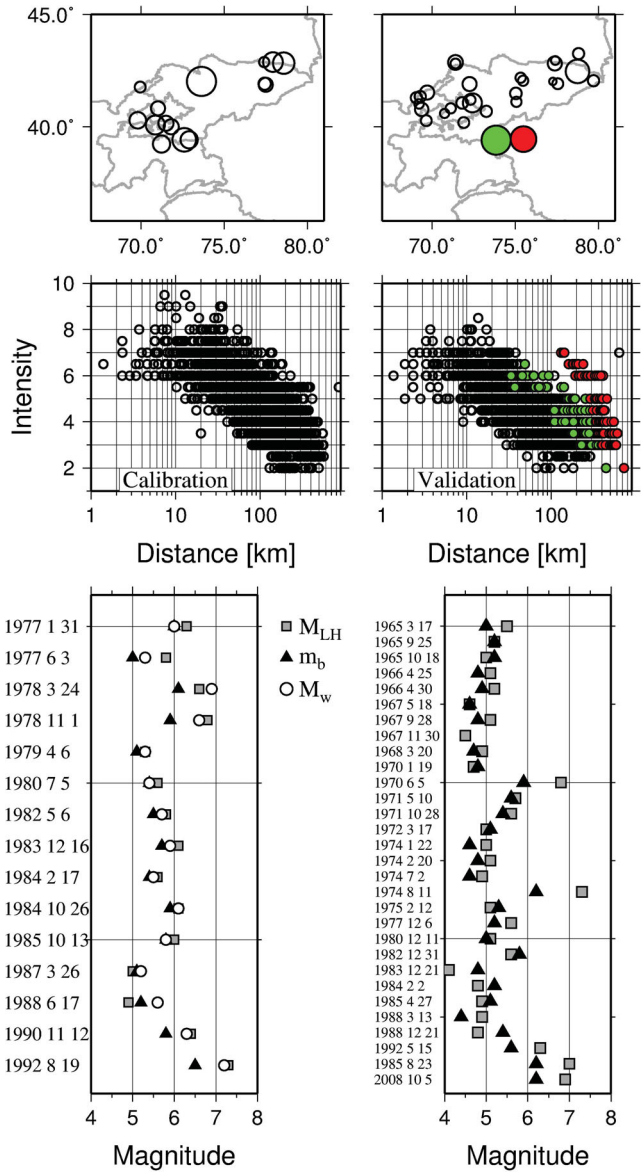

Figure 3. The calibration (left-hand panel, Table 1) and validation (right-hand panel, Table 2) data sets. Top panel: epicentres of the considered earthquakes. Middle panel: intensity versus epicentral distance scatter-plots. Bottom panel: magnitudes as compiled from different catalogue (M_{LH} from CASRI, m_{b} from ISC and M_{w} from GCMT). In the top panels, the symbol size is proportional to M_{LH}. The red and green circles indicate the epicentral locations (top right-hand panel) and the intensity values versus distance (middle right-hand panel) of the 1985 August 23 (ID 75 in Table 2) and 1974 August 11 (ID 71 in Table 2) earthquakes, respectively.

The model is then inverted to estimate the single-site magnitude MI_{ij} (with $i = 1,\ldots,P_j$ where P_j is the total number of intensity values available for the jth earthquake) from individual intensity values I_{ij} observed at distances Δ_{ij}

$$\mathrm{MI}_{ij} = \frac{1}{c_1}\left[I_{ij} - c_0 - c_2 \log_{10}(\Delta_{ij}) - c_3 \Delta_{ij}\right]. \quad (2)$$

Hereinafter, we indicate with MI (intensity magnitude) the magnitude estimated from intensity. In the second step of BW97, the location and magnitude of a given earthquake j are estimated by computing the intensity magnitude $\mathrm{MI}^k{}_{ij}$ over a grid of trial epicentre locations x_k. The magnitude $\mathrm{MI}^k{}_j$ is defined as the average of the

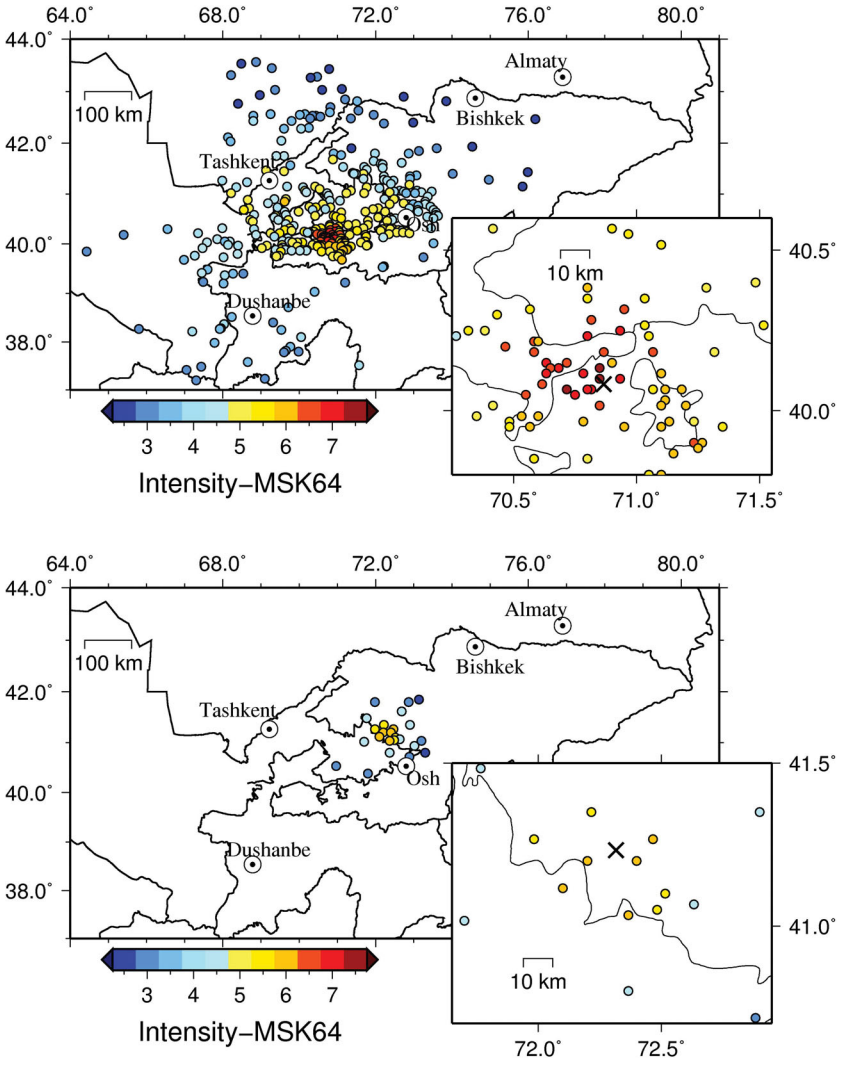

Figure 4. Top panel. Spatial distribution of 359 available intensity values for the ID = 54 earthquake ($M_{LH} = 6.3$, Table 1). Bottom panel. Distribution of 89 available intensity values for the ID = 63 earthquake ($M_{LH} = 4.8$, Table 2). Intensities and epicentres (black cross) are taken from Januzakov *et al.* (2003).

magnitudes $MI^k{}_{ij}$ estimated from individual intensity observations for earthquake j and assuming that the epicentre is located in $\mathbf{x}_k$, that is

$$MI^k_j = \frac{1}{P_j}\sum_{i=1}^{P_j} MI^k_{ij}. \tag{3}$$

Then, considering a grid of trial epicentres $\mathbf{x}_k$, the root mean square rms($MI^k{}_j$) is computed as

$$\mathrm{rms}(MI^k_j) = \left[\frac{1}{\sum_i w_i^2}\sum_i w_i \left(MI^k_{ij} - MI^k_j\right)^2\right]^{1/2}, \tag{4}$$

where W_i is a distance weighting function

$$W_i = \begin{cases} 0.1 + \cos\left[(\Delta_i/150)\times\pi/2\right] & \text{for}\Delta_i < 150\text{km} \\ 0.1 & \text{for}\Delta_i \geq 150\text{km} \end{cases}. \tag{5}$$

Finally, an offset equal to the minimum of rms($MI^k{}_j$) with respect to k is applied to rms($MI^k{}_j$).

According to Bakun & Wentworth (1997) and Bakun (1999), the intensity centre (IC) for earthquake j is the trial epicentre $\bar{x}_k$ for which rms(MI) is minimum, whereas the intensity magnitude MI_j is given by $MI_j{}^k$ evaluated at the IC point.

Modified Bakun and Wentworth approach

In this study, the BW97 approach is applied to Central Asia with some modifications. The main modification concerns the calibration of the attenuation model (1). In this study, a non-parametric approach is followed (e.g. Bindi *et al.* 2011; Oth *et al.* 2011), where the intensity values are expressed in terms of a source (α) and attenuation (β) term

$$I_{ij} = \alpha_j + \phi_l\beta_l + (1-\phi_l)\beta_{l+1}, \tag{6}$$

where $i = 1,\ldots,N_{\text{data}}$ indicates the ith intensity observation, $j = 1,\ldots,N_{\text{eq}}$ indicates the jth earthquake, $l = 1,\ldots,N_{\text{bin}}+1$ indicates a distance value r_l selected such that the hypocentral distance Δ_{ij} is within a bin defined by $r_l \leq \Delta_{ij} \leq r_{l+1}$. The attenuation function is linearized between r_j and r_{j+1} using the weights ϕ, computed as $\phi_l = (r_{l+1} - \Delta_{ij})/(r_{l+1} - r_l)$. In this application, the distance range 0–600 km in discretized into 30 intervals equal spaced over a logarithm distance scale. It is worth noting that this discretization is relevant to the attenuation model while the intensity assignments

are not processed through any binning scheme (e.g. Bakun & Scotti 2006). Model (6) moreover assumes that the attenuation is independent of the earthquake's size and is only a function of distance.

The parameters α_j and β_l are determined by performing a least-squares fit over a set of observations. To remove the trade-off between the source and attenuation terms, the attenuation function is constrained to assume a unit value at 25 km (e.g. Oth *et al.* 2008). There are two main advantages in using the non-parametric approach. First, the source term is not tied to any particular measure of the size of an earthquake (i.e. to a particular magnitude scale). When different magnitudes are included in the calibration data set, this approach allows different magnitudes to be assigned to historical earthquakes using the same attenuation model. Secondly, the attenuation is described in a tabular form without assuming any *a priori* model for the decay of the intensity values with distance. To estimate the uncertainties affecting the attenuation and source models, the regression analysis is repeated over 400 bootstrap replications of the original data set while computing the average and standard deviation of the distribution populated by the bootstrap results (e.g. Efron 1979). Each replication is a data set having the same number of elements as the calibration data set, but constructed by randomly selecting with replacement elements (i.e. intensity values) from the calibration data set. Tests performed with higher number of bootstrap replications confirmed that 400 replications are enough to reach a convergence of the results.

Regarding the second step, we follow the scheme of BW97, but consider $\alpha^{\kappa}{}_j$ instead of $\mathrm{MI}^{\kappa}{}_j$ and selecting the IC by minimizing $\mathrm{rms}(\alpha^{\kappa}{}_j)$ over a grid of trial epicentres, analogous to eq. (4). In this study, a grid spacing of 0.05° is considered in both the latitude and longitude directions.

Finally, following previous works (e.g. Bakun 2006; Bakun & Scotti 2006), bootstrap replications of the original data set are considered to estimate the uncertainties associated with the intensity locations and magnitudes. In particular, the 2.5th and 97.5th percentiles (i.e. considering a 5 per cent confidence interval) of the magnitude distribution obtained by analysing 400 bootstrap replications are taken to be the confidence interval for the estimated magnitudes MI_j. The extension of the area defined by the bootstrap epicentre solutions is estimated by evaluating the 67th and 95th percentiles of the distribution of distances from each epicentre to their centroid.

Finally, it is worth noting that in BW97, intensity binning is applied, where the median for all sites assigning the same intensity is taken to represent the central tendency of the assignments for that intensity level. Moreover, a set of site corrections, evaluated as the average residual for each location, is subtracted from the intensity assignments before applying the grid search. In this work, we do not attempt to reduce the uncertainties associated with IC and MI by reducing the data and residual variances using these assumptions. Therefore, we analyse the intensity data points without applying any binning scheme.

CALIBRATION

We consider the 15 calibration earthquakes listed in Table 1 to derive an attenuation model for the whole study region. We investigated the existence of regional effects affecting the attenuation of intensity values with distance by considering three subareas that are homogeneous from a deformation point of view (see Appendix). Considering the relatively small size of the analysed data set, a more detailed refinement would not produce robust results. The results, reported in the Appendix, show that with this data set, the consideration of more detailed regional models is not supported.

Fig. 5 presents the non-parametric model derived considering the calibration events. The attenuation with distance parameter derived considering the epicentres listed in the ISC catalogue and fixing the depth to 10 km is shown in Fig. 5(a) (red circles). The vertical bars represent the standard deviation estimated through the bootstrap analysis. For the sake of comparison, Fig. 5(a) also shows the average models derived fixing the depth to 20 km (grey triangles) and considering for each earthquake the actual depth listed in the ISC catalogue (black squares). The models show a reasonable agreement and only the model derived considering the ISC depths shows an early saturation at short distances. In addition, Fig. 5 shows that the non-parametric models agree well with the parametric attenuation function (blue line) recently obtained for Central Asia by Bindi *et al.* (2011). The latter has been derived considering a catalogue of 66 earthquakes, including the calibration and validation earthquakes considered in this study and considering the magnitudes and locations according to the CASRI catalogue.

In the panels (b) through to (f) of Fig. 5, the source terms α_j (see eq. 6) are regressed against different measures of earthquake magnitude, that is: surface wave magnitude M_{LH} from the CASRI catalogue (panel b), body-wave magnitude m_{b} from the ISC catalogue (panel c), moment magnitude M_{w} from GCMT (panel d), surface wave magnitude M_{s} from GCMT (panel e) and K-class from the CASRI catalogue (panel f). In all cases, a Simple Orthogonal Regression (e.g. Bormann & Khalturin 1975; Ambraseys 1990) is performed and the resulting models describing α as a function of each magnitude measure are shown in each panel. These relationships are used to compute the magnitudes of the earthquakes for the different scales in the validation and application data sets. The α values will be obtained through a grid-search procedure applied to the intensities corrected for the non-parametric attenuation.

In Fig. 6, the residuals, computed as observations minus predictions from the derived non-parametric model, are shown plotted against M_{LH} and distance. The mean residual $\pm$ one standard deviation is evaluated over magnitude bins 0.5 wide (starting from magnitude 4.5) and over 10 distance bins equal-spaced over a logarithm scale from 10 to 400 km (plus one additional bin including all the intensities at distances <10 km) are also shown. The average residual is zero, with a sigma equal to 0.51, and the bias does not show any dependence on magnitude and distance. The interevent error (not shown here) is zero for all earthquakes with a standard deviation varying from 0.39 (event ID 22 in Table 1) to 0.61 (event ID 28).

In Fig. 7, as a preliminary test, the method is applied to one of the earthquakes included in the training set, that is the $M_{\mathrm{LH}} = 7.3$, 1992 Suusamyr earthquake. Despite its magnitude, this large earthquake occurred in a sparsely populated mountain area, causing minimal loss of life. The earthquake ruptured along the southwest side of the Suusamyr valley and it was followed by three large aftershocks with magnitudes m_{b} 6.0, M_{s} 6.6 and M_{s} 6.6, respectively (e.g. Mellors *et al.* 1997), occurring within 2 hr of the main shock (ISC catalogue). The epicentres of these aftershocks are indicated with red stars in Fig. 7 (bottom panel). Previous studies highlighted the elliptical shape of the isoseismal map constructed from the intensity data points, whose east–west elongation is consistent with the trend of the major geological features in the area (e.g. Ghose *et al.* 1997). The asymmetry in the felt area, with large intensities extending farther to the west than to the east, has been attributed to either rupture directivity effects (e.g. Ghose *et al.* 1997) or to the superposition of the effects generated by the

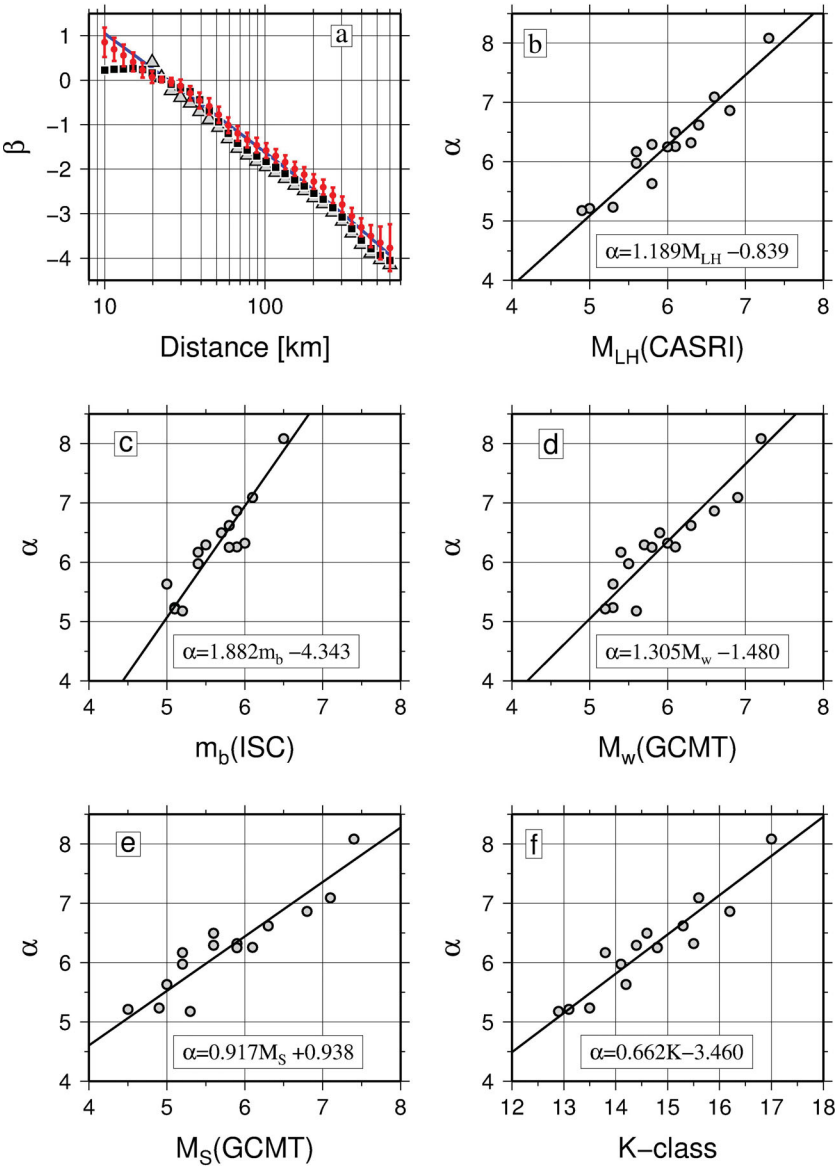

Figure 5. Panel (a). Average non-parametric attenuation arising for $h = 10$ km (red circles), $h = 20$ km (grey triangles) and h equal to the depth listed in the ISC catalogue for each earthquake (black squares). For the case $h = 10$ km, the red vertical bars represent the 95 per cent confidence interval from bootstrap analysis. The models are compared to the parametric model of Bindi *et al.* (2011) (blue line). From panels (b) to (f), the non-parametric source model is compared to different measures of the earthquake size. In each case, the equation for the best fitting line (black line) is shown.

main shock to those related to the two largest aftershocks (e.g. Kalmetieva *et al.* 2009).

The IC of the main shock obtained from the use of the inferred non-parametric model, indicated with a black square in Fig. 7, is shifted about 15 km in a northwestern direction, towards the location of the seismic moment centroid taken from the GCMT catalogue (empty circle in Fig. 7, bottom panel) and close to the epicentre of the first aftershocks (m_b 6.0) which occurred a few minutes after the main shock. The magnitude MI_{LH} at the IC is equal to 7.52, with 5th and 95th percentiles from bootstrap analysis (Fig. 8) equal to [7.45; 7.61], slightly larger than $M_{LH} = 7.3$ used in the calibration. Some contour lines for MI_{LH} are shown in green in the bottom panel of Fig. 7. At the ISC epicentre (grey cross in Fig. 7), MI_{LH} is equal to 7.53, very similar to that at the IC. The grid nodes corresponding to the IC solutions obtained by analysing 400 bootstrap replications (grey squares) are distributed between the epicentres of the three aftershocks and are encompassed by the 0.05 rms(α^k) iso-line (some iso-lines are shown as red curves in Fig. 7, middle panel). The 67th percentile of the distribution of distances between each gridpoints corresponding to a bootstrap IC solution and their centroid is 7.5 km (which increases to 9.7 km when considering the 95th percentile), confirming that the solution is well constrained.

VALIDATION

The non-parametric model is now applied to estimate the locations and magnitudes of the validation earthquakes. Fig. 9 compares the obtained locations with those from the ISC. Except for one earthquake (i.e. the M_{LH} 7.0, 1985 Southern Xinjiang earthquake, shown in red symbols), the IC locations are in good agreement with the

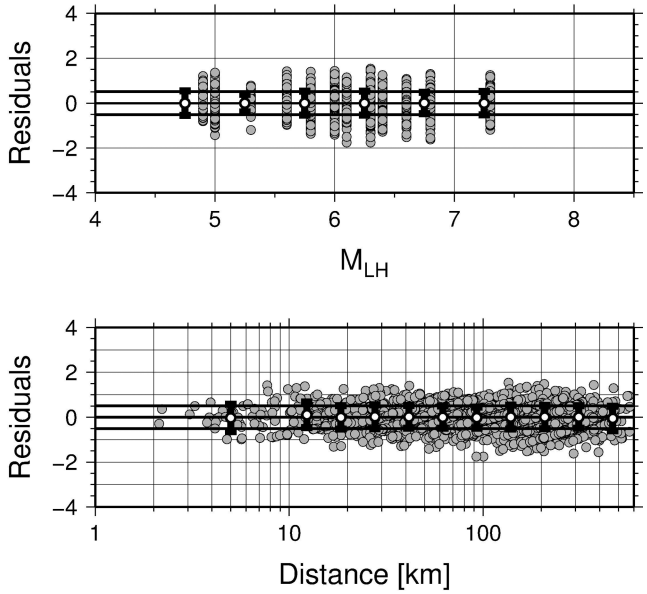

Figure 6. Residuals computed between values obtained using the non-parametric model versus both M_{LH} (top panel) and epicentral distance (bottom panel). The mean ± one standard residuals computed over magnitude bins 0.5 wide (top panel) and equal-spaced distance bins (except the first which includes distances less than 10 km) on a logarithm scale (bottom panel) are also shown. The horizontal black lines represent the average residual and the average ± sigma.

epicentres listed in the ISC catalogue, with most of the horizontal shift being less than 15 km, as shown by the histograms in Fig. 9. The comparisons between the magnitudes provided by the catalogues and those estimated at the IC points are shown in the bottom panels (see also Table 3). The values of the body wave intensity magnitude mI_b are in good agreement with m_b provided by ISC, with differences within ±0.5 magnitude units (m.u.). A good agreement is also observed between MI_{LH} and M_{LH}, although two earthquakes show a difference greater than 0.75 m.u. The spatial distribution of the magnitude differences is shown in the bottom panel. The absence of any pattern in the distribution of positive or negative residuals suggests that the differences between instrumental and intensity magnitudes are not biased by the attenuation model, in agreement with the discussions presented in the Appendix.

To check the influence of assumptions dealing with the depth values, we also compute the magnitudes considering models calibrated for a fixed depth equal to 20 km as well as considering for each earthquake the depths listed in the ISC catalogue. The differences among the obtained magnitudes, shown in Fig. 10, are negligible, confirming our assumption that the depth values are not critical for the methodology applied in this study.

Finally, we present the results for the 1985 Southern Xinjiang (ID = 75, Table 2) and 1974 Markansu (ID = 71, Table 2) earthquakes, which show large differences in the location (the former) and magnitude (the latter) estimations from intensity with respect to the instrumental information, as well as the 2008 Nura earthquake (ID = 90, Table 2).

The M_{LH} 7.0, 1985 Southern Xinjiang earthquake

The largest difference in location is observed for the 1985 Xinjiang earthquake. The IC is shifted to the northwest by about 140 km, close to the border between Kyrgyzstan and China. Although the

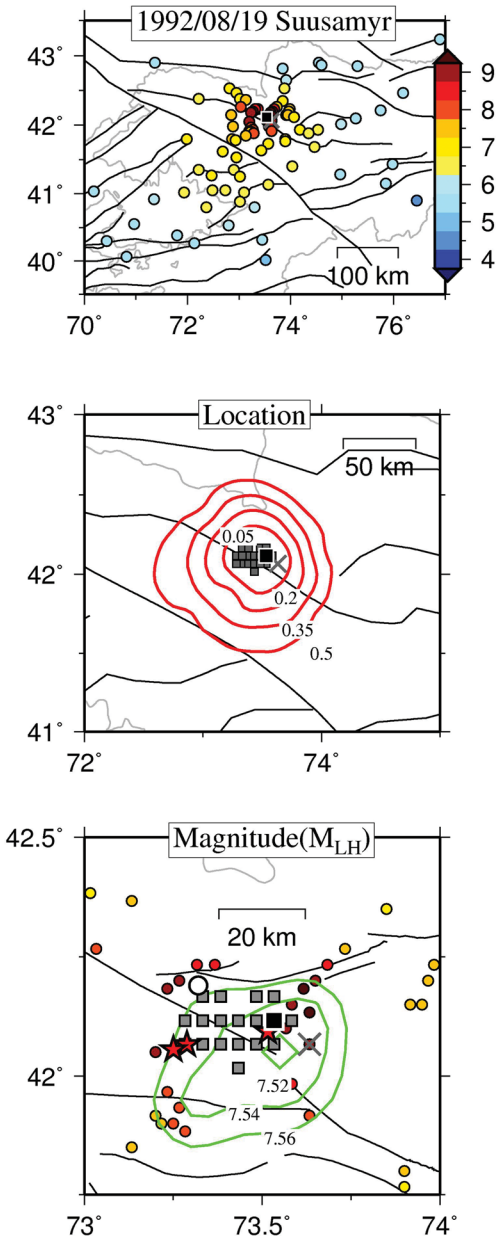

Figure 7. Top panel: intensity values for the 1992, M_{LH} 7.3 Suusamyr (Kyrgyzstan) earthquake. The ISC epicentre location is indicated with a grey cross, the IC with a black square. Middle panel: contour lines (red) of rms(α^k) and distribution of the ICs obtained from the bootstrap analysis (grey squares). Bottom panel: M_{LH} magnitude contour lines (grey), epicentres of three large aftershocks (red stars), location of the GCMT solution (empty circle), nodes of the trial-location grid corresponding to the bootstrap solutions (grey squares) and the obtained IC (black square). The main active faults are sketched as black lines.

BW97 approach could fail in locating an earthquake outside the area covered by felt intensities (e.g. Bakun 2000), the IC location would produce an intensity-distance distribution more compatible with those of the other earthquakes (see the grey circles in the middle-right panel of Fig. 3, where the distances are computed from the ISC epicentre). Moreover, the magnitudes estimated for the IC are in good agreement with those provided by the catalogues. For example, the estimated MI_{LH} and MI_b are 7.02 and 6.29, respectively, close to the values of 7 and 6.2 provided by the

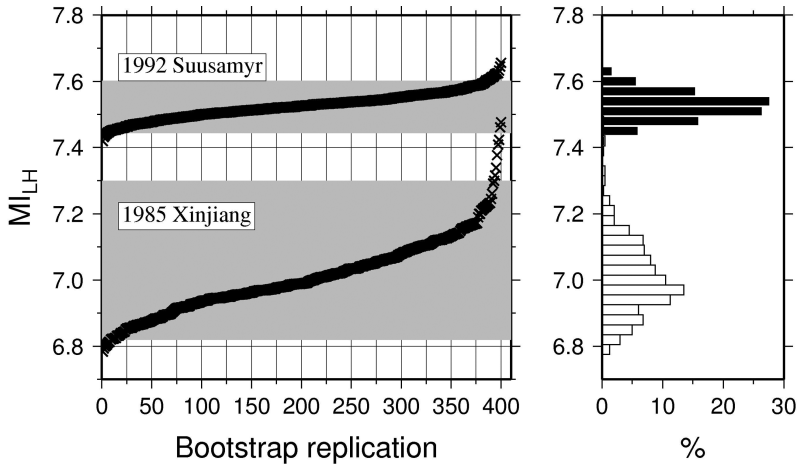

Figure 8. Magnitude distributions from the bootstrap analysis performed for two earthquakes discussed in the text. Left panel: Crosses are the magnitudes evaluated at the IC for different bootstrap runs, the grey areas are limited by the 5th and 95th percentiles of the distributions. Right-hand panel: histograms of the magnitude values obtained via bootstrap analysis for the 1992 Suusamyr (black) and 1985 Xinjiang (white) earthquakes.

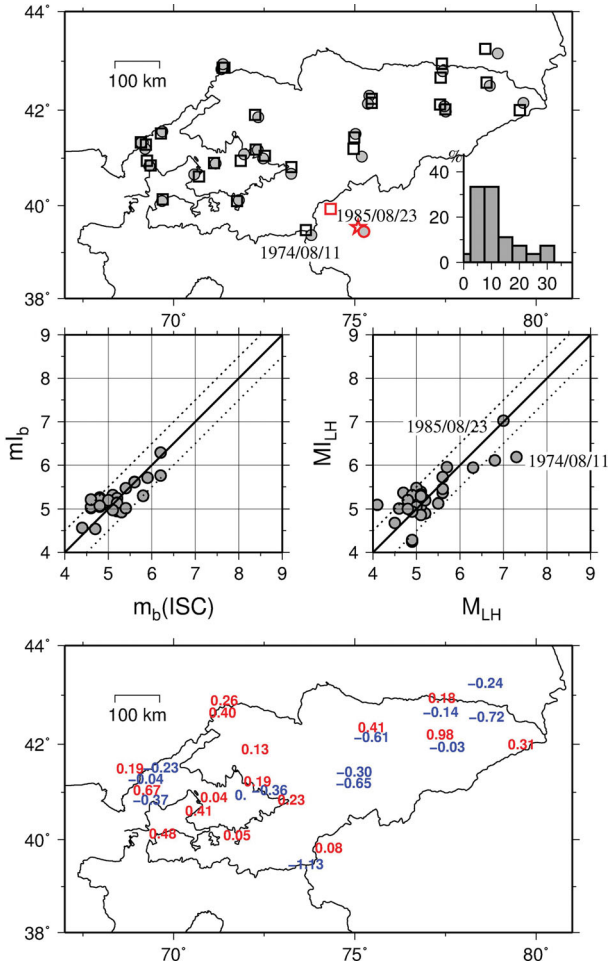

Figure 9. Results of the validation test. Top panel. ISC locations (circles) and obtained IC points (squares). The histogram of the distances (in km) between the two locations is also shown, excluding the 1985 Southern Xinjiang earthquake (ID = 75, Table 2). Regarding the Southern Xinjiang earthquake, the star represents the moment centroid provided by GCMT. Middle. Magnitudes m_b (left-hand panel) and M_{LH} (right-hand panel) compared with those estimated at the IC. The one-to-one (black) ±0.5 magnitude units (dotted) lines are shown for comparison. Bottom panel: spatial distribution of the differences between the obtained macroseismc (MI_{LH}) and instrumental (M_{LH}) magnitudes (positive differences are shown in red, negative in blue).

CASRI and ISC catalogues. The 5th and 95th percentiles of the bootstrap distribution for MI_{LH} (Fig. 8) are 6.82 and 7.25, respectively, whereas at the instrumental epicentre, the intensity magnitudes are $MI_{LH} = 7.46$ and $MI_b = 6.56$, larger than the instrumental ones.

This situation is different from that described by Bakun (2000), who analysed earthquakes that occurred off-shore of California's north coast. The author showed that it was not possible to constrain intensity locations and magnitudes simultaneously, but, when the intensity magnitude was evaluated at the instrumental epicentre, it assumed values close the instrumental ones. For the southern Xinjiang earthquake, the intensity location is far from the epicentre, but the intensity magnitude at the IC is similar to the instrumental one. Although the bootstrap solutions for the IC lie within the 0.05 rms contour line, the area included by this line is very wide (for comparison, see the results obtained for the 1992 Suusamyr earthquake shown in Fig. 8). In particular, the 67th percentile of the distribution of distances between gridpoints corresponding to bootstrap solutions for IC and their centroid is 21 km (which increases to 40 km when the 95th percentile is considered), indicating that the minimum of the grid search does not well constrain the solution, as confirmed also by the largest difference (0.47) between the 97.5th and 2.5th percentiles of the bootstrap magnitude distribution obtained for this earthquake (Table 3).

Finally, it is worth noting that the same discrepancy is observed when the attenuation models obtained assuming different depths are used.

The m_b 6.2, 1974 Markansu and the M_w 6.7, 2008 Nura earthquakes (Tajikistan)

The 1974 Markansu earthquake occurred in a structurally complex region along the Main Pamir Thrust fault zone, generated by the India-Eurasia convergence. The focal mechanism of this earthquake and that of its main aftershocks has been studied in several publications, reaching different conclusions. Due to a lack of field data in the epicentral region, Ni (1978) observed from LANDSAT images that this earthquake occurred in a region of northeast trending structures dipping steeply to the south and after analysing about 200 first polarities, proposed an oblique thrusting mechanism. Later, Jackson *et al.* (1979) revised some of the polarities and obtained

Table 3. The locations (IC) and magnitudes (MI) of the validation earthquakes as obtained in this study. The 2.5–97.5 per cent confidence interval for the magnitudes is also listed. Δ_{67} and Δ_{95} indicate the 67th and 95th percentiles of the distribution of distances between each bootstrap solution for the IC and their centroid.

ID	Lat IC	Lon IC	Δ_{67} [km]	Δ_{95} [km]	MI_{LH}	[2.5–97.5] per cent		mI_b	[2.5–97.5] per cent		MI_S	[2.5–97.5] per cent		MI_W	[2.5–97.5] per cent		KI	[2.5–97.5]	
45	69.37	40.85	8	25	5.1	5.0	5.3	5.1	5.0	5.2	4.7	4.6	5.0	5.1	5.1	5.3	13.1	13.0	13.5
12	74.98	41.43	4	10	4.9	4.8	5.0	4.9	4.9	5.0	4.4	4.2	4.6	4.9	4.8	5.1	12.7	12.5	12.9
13	77.5	42.02	9	18	5.0	4.8	5.1	5.0	4.9	5.1	4.5	4.3	4.6	5.0	4.9	5.1	12.8	12.6	13.1
46	69.23	41.28	6	12	5.1	5.0	5.2	5.1	5.0	5.1	4.6	4.5	4.8	5.1	5.0	5.2	13.0	12.9	13.2
47	71.85	40.95	4	10	5.2	5.1	5.3	5.1	5.1	5.2	4.8	4.7	4.9	5.2	5.1	5.3	13.3	13.1	13.5
48	70.7	40.62	7	12	5.0	4.9	5.1	5.0	5.0	5.1	4.5	4.4	4.7	5.0	4.9	5.2	12.9	12.7	13.1
14	79.55	42	17	45	5.4	5.2	5.5	5.3	5.1	5.4	5.0	4.7	5.2	5.4	5.2	5.5	13.6	13.2	13.9
15	77.4	42.95	10	20	4.7	4.5	5.3	4.8	4.7	5.2	4.1	3.9	4.9	4.7	4.6	5.3	12.3	12.1	13.4
16	74.97	41.2	4	9	4.2	4.1	4.4	4.5	4.4	4.7	3.6	3.3	3.8	4.4	4.2	4.5	11.6	11.2	11.9
49	69.27	40.95	5	9	5.4	5.2	5.5	5.2	5.2	5.3	5.0	4.8	5.2	5.4	5.3	5.5	13.6	13.3	13.8
17	78.63	42.57	2	5	6.1	6.1	6.2	5.7	5.7	5.8	6.0	5.9	6.1	6.0	6.0	6.1	14.9	14.8	15.1
18	71.4	42.87	5	8	6.0	5.9	6.0	5.6	5.6	5.7	5.8	5.7	5.9	5.9	5.8	6.0	14.6	14.5	14.7
50	72.25	41.9	18	32	5.7	5.6	5.9	5.5	5.4	5.6	5.5	5.4	5.6	5.7	5.6	5.8	14.2	14.0	14.4
51	69.7	40.13	7	10	5.5	5.4	5.5	5.3	5.3	5.4	5.1	5.1	5.2	5.5	5.4	5.5	13.8	13.7	13.9
52	71.75	40.1	5	16	5.1	4.9	5.2	5.0	4.9	5.2	4.6	4.4	4.8	5.1	4.9	5.2	13.0	12.7	13.3
53	73.25	40.82	6	10	5.3	5.2	5.4	5.2	5.1	5.3	5.0	4.8	5.1	5.3	5.2	5.4	13.5	13.3	13.7
19	75.47	42.23	4	7	5.3	5.1	5.5	5.2	5.1	5.3	4.9	4.7	5.1	5.3	5.1	5.5	13.5	13.1	13.8
71	73.65	39.48	15	39	6.2	6.0	6.4	5.8	5.6	5.9	6.1	5.8	6.3	6.1	5.9	6.3	15.0	14.7	15.3
20	78.6	43.25	6	10	4.9	4.7	5.0	4.9	4.9	5.0	4.3	4.2	4.5	4.9	4.8	5.0	12.7	12.4	12.8
56	69.65	41.52	3	6	5.4	5.3	5.4	5.2	5.2	5.3	5.0	4.9	5.1	5.4	5.3	5.4	13.6	13.4	13.7
57	69.1	41.33	4	5	5.3	5.2	5.4	5.2	5.1	5.3	4.9	4.8	5.0	5.3	5.2	5.4	13.4	13.3	13.6
24	77.37	42.67	7	10	5.5	5.4	5.5	5.3	5.3	5.3	5.1	5.0	5.2	5.4	5.4	5.5	13.7	13.6	13.8
25	77.35	42.12	8	10	5.1	5.0	5.2	5.1	5.0	5.1	4.7	4.5	4.8	5.1	5.0	5.2	13.1	12.9	13.3
26	71.35	42.87	8	12	5.2	5.1	5.4	5.1	5.1	5.2	4.8	4.7	5.0	5.2	5.1	5.4	13.3	13.1	13.5
60	71.17	40.9	3	6	4.9	4.8	5.1	5.0	4.9	5.1	4.4	4.2	4.6	5.0	4.8	5.1	12.8	12.5	13.1
27	75.47	42.15	3	7	4.3	4.2	4.4	4.6	4.5	4.6	3.6	3.5	3.8	4.4	4.3	4.5	11.6	11.4	11.9
63	72.27	41.18	8	13	5.0	4.8	5.2	5.0	4.9	5.1	4.5	4.2	4.8	5.0	4.8	5.2	12.9	12.5	13.2
64	72.52	41.05	4	8	5.9	5.7	6.1	5.6	5.5	5.7	5.7	5.5	6.0	5.9	5.7	6.1	14.6	14.2	14.9
75	74.33	39.93	22	40	7.0	6.8	7.2	6.3	6.2	6.4	7.1	6.9	7.5	6.9	6.7	7.1	16.5	16.2	16.9
90	74.75	39.58	12	28	6.2	5.8	6.3	5.8	5.5	5.9	6.1	5.6	6.3	6.1	5.8	6.3	15.1	14.4	15.3

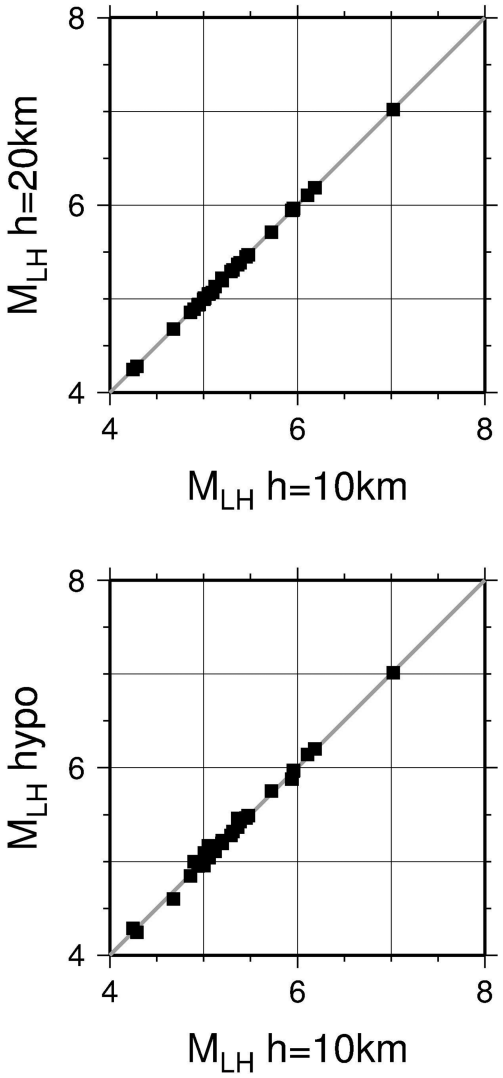

Figure 10. Top panel: M_{LH} magnitudes of the validation earthquakes obtained by considering the model for a fixed depth equal to 20 km against those for depths fixed to 10 km. Bottom panel: The same as the top, but considering the magnitudes obtained for a model calibrated using the depths as listed in the ISC catalogue.

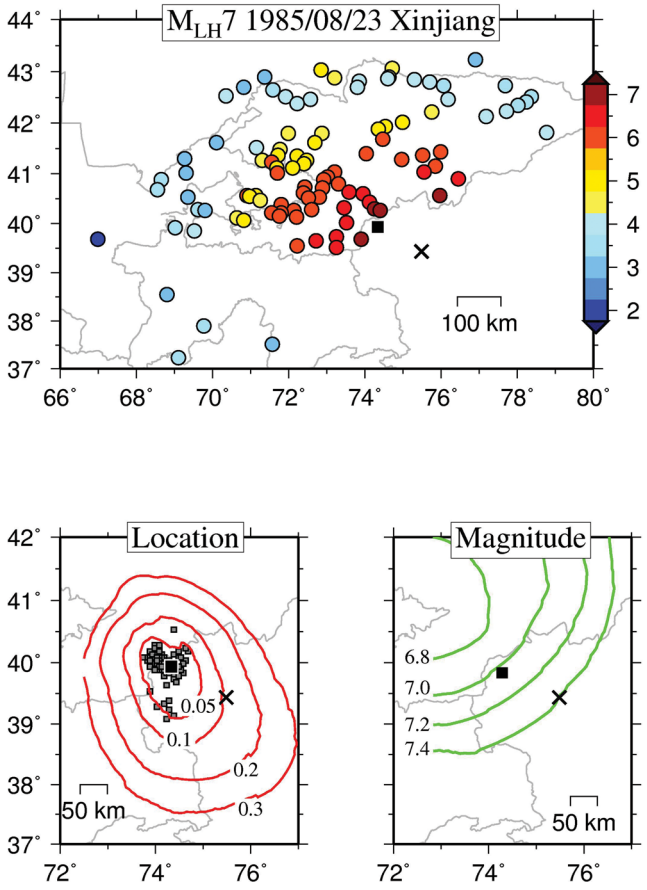

Figure 11. Analysis for the 1985 Southern Xinjiang earthquake (ID = 75 in Table 2). Top panel: intensity values, epicentral location as in the CASRI catalogue (cross) and final IC location (square). Bottom left-hand panel: contour lines (red) of rms(α^k) and distribution of the ICs obtained with the bootstrap analysis (grey squares) are shown. Bottom right-hand panel: contour lines (green) for MI_{LH}.

a strike-slip solution, proposing also a multiple rupture hypothesis where the true first arrival is small and hence nodal at most stations with later arrivals associated with a later rupture with a different orientation. Finally, Langston & Dermengian (1981) performed a robust evaluation of the focal mechanism, considering also waveform modelling of both *P* and *S* phases, to account for the effects of strong model-related phases. Their preferred solution was a pure thrust event with a strike of 77° and a dip of 32°.

Fig. 12 (left) shows the analysis performed for the 1974 Markansu earthquake. The IC is located about 20 km northwest of the epicentre listed by ISC. The bulk of the 400 bootstrap locations lie within the 0.05 rms(MI) contour line, which has a spatial extent smaller than the area obtained for the southern Xinjiang earthquake, confirming that the location is better constrained (the 67th percentile of the distance distribution from the centroid is 15.1 km, the 95th percentile is 38.5 km). The bottom left panel of Fig. 12 shows the contouring line for MI_{LH}. At the IC, the estimated magnitude is 6.19 and the 2.5–97.5 per cent confidence interval is 6.0–6.35 (Table 3, ID = 71). Considering mIb, the 2.5–97.5 per cent confidence interval is 5.65–5.87, and the value inferred at the IC is 5.76, whereas the MI_w evaluated at the IC is $M_w = 6.12$, with a confidence interval of 5.95–6.27. These intensity magnitude values are less than those provided by the CASRI catalogue ($M_{LH} = 7.3$) and from ISC ($m_b = 6.2$). It is interesting to note that the IC moves closer to the epicentre of the 2008 Nura earthquake (shown asan empty circle in Fig. 11).

The Nura earthquake occurred close to the border among Kyrgyzstan, Tajikistan and China and caused about 70 fatalities. The earthquake and the aftershock sequence were well recorded by a temporary network (Krumbiegel *et al.* 2011) and the preferred focal solution for the main shock is a pure thrust event over a steep (55°) south-dipping plane. An incomplete data set of intensity points has been retrieved (Fig. 12, right), with values only inform Kyrgyzstan. Nevertheless, the IC location is quite stable, with bootstrap locations encompassed by the 0.1 rms(MI) contour line, except for those bootstrap replications where the intensity assignments closest to the epicentre were not selected (in that case the solution migrated towards the northwest). Regarding the intensity magnitudes, smaller values are obtained with respect to those in the catalogues (Table 3, ID = 90). In particular, MI_{LH} is 6.22, with the 5–95 per cent interval giving [5.81–6.33], whereas the value reported in CASRI is $M_{LH} = 6.9$. The value of MI_b is 5.78 with a confidence interval of [5.52–5.86] and MI_w is 6.14, with a confidence interval of [5.77–6.25],

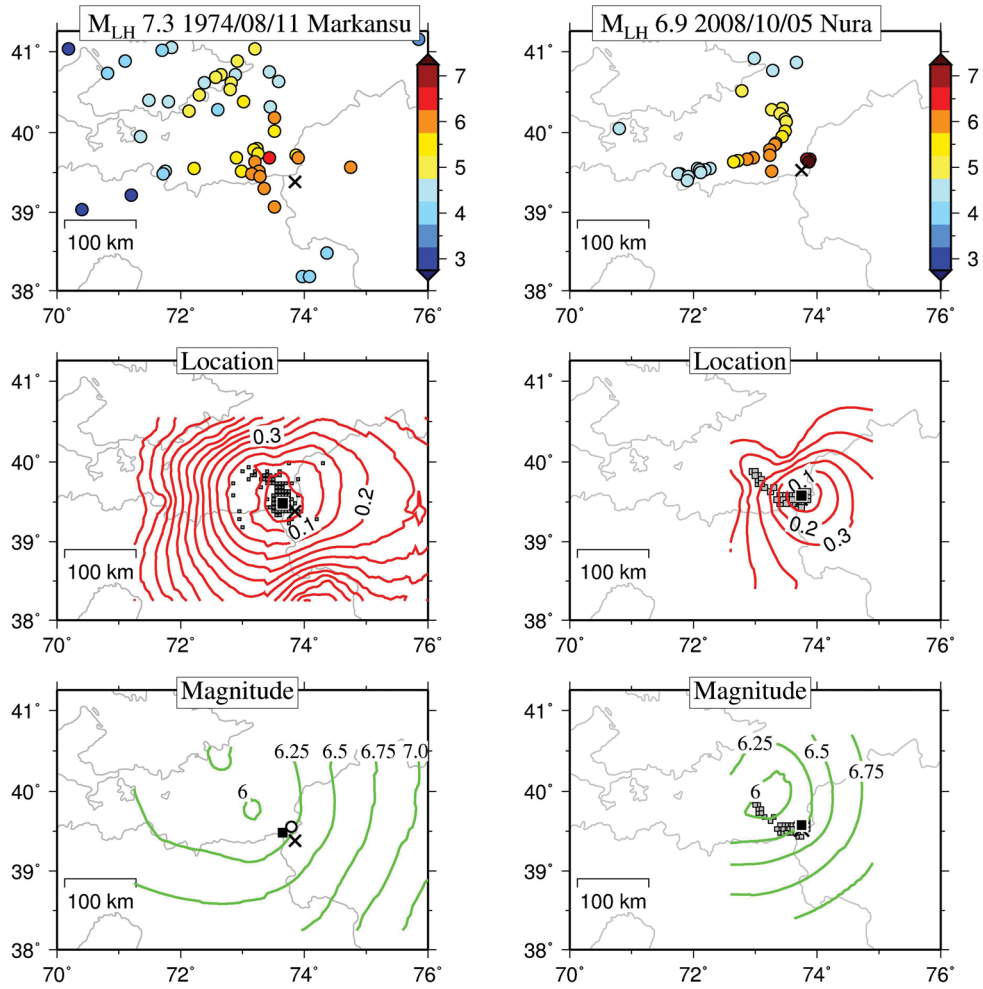

Figure 12. Validation earthquakes. (left-hand panel) Results obtained for the 1974 Markansu earthquake (ID = 71 in Table 2). Right-hand panel: 2008 Nura earthquake (ID = 90 in Table 2).

whereas the values reported in the ISC and GCMT catalogues are $m_b = 6.2$ and $M_W = 6.7$, respectively.

DISCUSSION AND CONCLUSIONS

We have applied a modified version of the Bakun & Wentworth (1997, 1999) method to estimate epicentral locations and magnitudes of earthquakes in Central Asia from intensity assignments. We introduced a non-parametric approach that allowed us to derive a model independent of any specific magnitude scale. The model has been calibrated using the intensity values associated with 15 earthquakes, while considering the epicentral locations listed in the ISC catalogue. The obtained non-parametric description of the earthquake sources have been in turn regressed with respect to different magnitude values as provided by different catalogues, namely M_w by CGMT, M_s by ISC and M_{LH} by the CASRI catalogue.

The validation of the model, performed over 30 earthquakes, showed that the intensity magnitude mI_b and the instrumental magnitude m_b agree within a difference of ±0.5 m.u (the distribution of differences has a median and standard deviation equal to 0.079 and 0.30, respectively). A slightly larger variability was obtained for M_{LH}, with differences within ±0.75 m.u. (the median difference is 0.038 with standard deviation equal to 0.44) except for two earthquakes (ID = 71 and 25, Table 2).

The uncertainties in the magnitudes estimated through bootstrap analysis are shown in Table 3. For MI_{LH}, the difference between the 97.5th and 2.5th percentiles of the magnitude distribution ranges between 0.11 and 0.75, with a median of 0.24 and a standard deviation of 0.13. Smaller differences are obtained for mI_b, from 0.07 to 0.48, with a median and standard deviation to 0.15 and 0.08, respectively. The validation test confirmed the overall reliability of the calibrated model although a significant discrepancy with respect to the instrumental magnitude is observed for the 1974 Markansu earthquake. This earthquake occurred along the border between Kyrgyzstan, Tajikistan and China, in an area not surrounded by intensity values, since those in the Tarim basin (China) are generally lacking in the available reports and the few values available towards the south are located in the Pamir area, at distances greater than 100 km. Although it is known that the Bakun and Wentworth method could fail in locating the epicentre for such a distribution of intensity values (Bakun 2000), the results from this study are somehow unexpected. If the origin of the discrepancy lies in the distance-magnitude trade-off, by fixing one of the two unknowns, the other should be resolvable. Bakun (2000) showed that it was not possible to obtain simultaneously reliable locations and magnitudes for earthquakes that occurred off-shore, but when the intensity

magnitude was evaluated at the instrumental epicentre, the obtained value agreed with the instrumental magnitude. In our case, we obtained either a IC location consistent with the epicentre, but with an intensity magnitude less than the instrumental one (Markansu and Nura earthquakes), or an intensity magnitude close the instrumental one, but with a IC location considerably offset from the instrumental epicentre (southern Xinjiang earthquake). This problem is similar to that encountered for a number of test cases in India (Szeliga *et al.* 2010).

For the Southern Xinjiang earthquake, the ISC epicentre is very close to both the CASRI epicentre (Table 1) and to the moment centroid provided by GCMT (indicated with a star in the map of Fig. 9). Since all the instrumental locations are in good agreement, further investigations into the intensities available are needed to understand the origin of the discrepancy between the IC location and the instrumental epicentre.

Finally, the application of the model calibrated in this work to 31 earthquakes that occurred earlier than 1964 is ongoing. The results for these earthquakes, presented in a separate paper, will be compared to magnitude and locations determined following the standard procedure as applied in the former Soviet Union (e.g. Kondorskaya & Shebalin 1982).

ACKNOWLEDGMENTS

This work has been carried out within the EMCA-Earthquake Model Central Asia (http://www.emca-gem.org) and Global Seismic History (www.nexus.globalquakemodel.org/global-earthquake-history/) projects. Comments from W. Bakun, R. Bilham, an anonymous reviewer and E. Fukuyama (Editor) are gratefully acknowledged. We also thank K. Fleming for improving the English of our paper.

REFERENCES

Abdrakhmatov, K., Havenith, H.-B., Delvaux, D., Jongmans, D. & Trefois, P., 2003. Probabilistic PGA and Arias intensity maps of Kyrgyzstan (Central Asia), *J. Seismol.,* **7,** 203–220.

Alvarez-Rubio, S., Kästli, P., Fäh, D., Sellami, S. & Giardini, D., 2011. Parameterization of historical earthquakes in Switzerland, *J. Seismol.,* **16,** 1–24.

Ambraseys, N.N., 1990. Uniform magnitude reevaluation of European earthquakes associated with strong-motion records, *Earthq. Eng. Struct. Dyn.,* **19,** 1–20.

Bakun, W.H. & Wentworth, C.M., 1997. Estimating earthquake location and magnitude from seismic intensity data, *Bull. seism. Soc. Am.,* **87,** 1502–1521.

Bakun, W.H., 1999. Seismic activity of the San Francisco Bay region, *Bull. seism. Soc. Am.,* **89,** 764–784.

Bakun, W.H. & Wentworth, C.M., 1999. Erratum to Estimating earthquake location and magnitude from seismic intensity data, *Bull. seism. Soc. Am.,* **89,** 557.

Bakun, W.H., 2000. Seismicity of California's north coast, *Bull. seism. Soc. Am.,* **90,** 797–812.

Bakun, W.H., 2006. Estimating locations and magnitudes of earthquakes in Southern California from modified Mercalli intensities, *Bull. seism. Soc. Am.,* **96,** 1278–1295.

Bakun, W.H. & Scotti, O., 2006. Regional intensity attenuation models for France and the estimation of magnitude and location of historical earthquakes, *Geophys. J. Int.,* **164,** 596–610.

Bakun, W.H., Gómez Capera, A. & Stucchi, M., 2011. Epistemic uncertainty in the location and magnitude of earthquakes in Italy from macroseismic data, *Bull. seism. Soc. Am.,* **100,** doi:10.1785/0120110118.

Beauval, C., Yepes, H., Bakun, W.H., Egred, J., Alvarado, Al. & Singaucho, J.-C., 2010. Locations and magnitudes of historical earthquakes in the Sierra of Ecuador (1587–1996), *Geophys. J. Int.,* **181,** 1613–1633.

Bindi, D., Parolai, S., Oth, A., Abdrakhmatov, K., Muraliev, A. & Zschau, J., 2011. Intensity Prediction Equations for Central Asia, *Geophys. J. Int.,* **187,** 327–337.

Bindi, D., Abdrakhmatov, K., Parolai, S., Mucciarelli, M., Grünthal, G., Ischuk, A., Mikhailova, N. & Zschau, J., 2012. Seismic hazard assessment in Central Asia: outcomes from a site approach, *Soil Dyn. Earthq. Eng.,* **37,** 84–91.

Bormann, P. & Khalturin, V.I., 1975. Relations between different kinds of magnitude determinations and their regional variations, in *Proceedings of the XIVth General Assembly of the European Seismological Commission Trieste, 16–22 September 1974,* Nationalkomitee für Geodäsie und Geophysik, AdK of the GDR, Berlin, pp. 27–35.

Bormann, P., 2002. Magnitude of seismic events, in *IASPEI, New Manual of Seismological Observatory Practice,* Vol. 1, pp. 16–50, ed. Bormann, P., GeoForschungsZentrum, Potsdam.

Burtman, V.S. & Molnar, P., 1993. Geological and geophysical evidences for deep subduction of continental crust beneath the Pamir, *Spec. Pap. Geol. Soc. Am.,* **281,** 76.

Choy, J.E., Palme, C., Guada, C., Morandi, M. & Klarica, S., 2010. Macroseismic interpretation of the 1812 earthquake in venezuela using intensity uncertainties and a priori fault-strike information, *Bull. seism. Soc. Am.,* **100,** 241–255.

Efron, B., 1979. Bootstrap methods, another look at the jackknife, *Ann. Stat*., **7,** 1–26.

Engdahl, E.R., van der Hilst, R.D. & Buland, R., 1998. Global teleseismic earthquake relocation with improved travel times and procedures, *Bull. seism. Soc. Am.,* **88,** 722–743.

Erdik, M., Rashidov, E., Safak, E. & Turdukulov, A., 2005. Assessment of seismic risk in Tashkent, Uzbekistan and Bishkek, Kyrgyz Republic, *Soil Dyn. Earthq. Eng.,* **25,** 473–486.

Evernden, J.F., 1975. Seismic intensities, size of earthquakes and related parameters, *Bull. seism. Soc. Am.,* **65,** 1287–1313.

Evernden, J.F., Kohler, W.M. & Clow, G.D., 1981. Seismic Intensities of Earthquakes of Conterminous United States—Their Prediction and Interpretation. U. S. Geological Survey Professional Paper 1223, 50 p.

Gasperini, P., Bernardini, F., Valensise, G. & Boschi, E., 1999. Defining seismogenic sources from historical earthquakes felt reports, *Bull. seism. Soc. Am.,* **89,** 94–110.

Gasperini, P., Vannucci, G., Tripone, D. & Boschi, E., 2010. The location and sizing of historical earthquakes using attenuation of macroseismic intensity with distance, *Bull. seism. Soc. Am.,* **100**(5A2), 035–2066.

Ghose, S., Mellors, R.J., Korjenkov, A.M., Hamburger, M.W., Pavlis, T.L., Pavlis, G.L., Mamyrov, E. & Muraliev, A.R., 1997. The $M_s = 7.3$ 1992 Suusamyr, Kyrgyzstan earthquake: 2. Aftershock focal mechanisms and surface deformation, *Bull. seism. Soc. Am.,* **87,** 23–38.

Gutenberg, B., 1945. Amplitudes of surface waves and magnitudes of shallow earthquakes, *Bull. seism. Soc. Am.,* **35,** 3–2.

Hanks, T.C., Hileman, J.A. & Thatcher, W., 1975. Seismic moments of the larger earthquakes of the southern California region, *Geol. Soc. Am. Bull.,* **86,** 1131–1139.

Jackson, J., Molnar, P., Patton, H. & Fitch, T., 1979. Seismotectonic aspects of the Markansu Valley, Tadjikistan, earthquake of August 11, 1974, *J. geophys Res.,* **84,** 6157–6167.

Januzakov, K.J., Omuraliev, M., Omuralieva, A., Ilyasov, B.I. & Grebennikova, V.V., 2003. *Strong Earthquakes of the Tien Shan (within the Kyrgyzstan Territory and Adjacent Regions of the Countries of Central Asia),* pp. 216, Ilim, Bishkek, ISBN 5-8355-1335-6.

Kalmetieva, Z.A., Mikolaichuk, A.V., Moldobekov, B.D., Meleshko, A.V., Jantaev, M.M. & Zubovich, A.V., 2009. *Atlas of Earthquakes in Kyrgyzstan,* Central Asian Institute for Applied Geosciences, Bishkek, ISBN 978-9967-25-829-7.

Karnik, V., 1962. Amplitude-distance curves of surface waves at short epicentral distances, *Stud. Geophys. Geod.,* **6,** 340–346.

Kondorskaya, N.V. & Shebalin, N.V., 1982. New Catalog of strong earthquakes in the U.S.S.R. from ancient times through 1977, in *National Oceanic and Atmospheric Administration,* pp. 608, eds. Kondorskaya, N.V. & Shebalin, N.V., Boulder, USA.

Krumbiegel, C., Schurr, B., Orunbaev, S., Rui, H. & Pingren, L., the TIPAGE Team, 2011. The 05/10/2008 Mw 6.7 Nura earthquake sequence on the Main Pamir Thrust, European Geophysical Union, General Assembly, Vienna, 3–8 April.

Langston, C.A. & Dermengian, C.M., 1981. Comment on 'Seismotectonic Aspects of the Markansu Valley, Tadjikstan, Earthquake of August 11, 1974' by James Jackson, Peter Molnar, Howard Patton, and Thomas Fitch, *J. geophys. Res,* **86,** 1091–1093.

Lukk, A.A., Yunga, S.L., Shevchenko, V.I. & Hamburger, M.W., 1995. Earthquake focal mechanisms, deformation state, and seismotectonics of the Pamir-Tien Shan region, Central Asia, *J. geophys. Res.,* **100**(B10), 20 321–20 343, doi:10.1029/95JB02158.

Medvedev, S., Sponheuer, W. & Kárník, V., 1964. Neue seismische Skala Intensity scale of earthquakes, 7. Tagung der Europäischen Seismologischen Kommission vom 24.9. bis 30.9.1962, In: Jena, Veröff. Institut für Bodendynamik und Erdbebenforschung in Jena, vol 77. Deutsche Akademie der Wissenschaften zu Berlin, pp. 69–76.

Mellors, R.J., Vernon, F.L., Pavlis, G.L., Abers, G.A., Hamburger, M.W., Ghose, S. & Iliasov, B., 1997. The $M_S = 7.3$ 1992 Suusamyr, Kyrgyzstan earthquake:1: constraints on fault geometry and source parameters based on aftershocks and body-wave modeling, *Bull. seism. Soc. Am.,* **87,** 11–22.

Mezcua, J., Rueda, J. & Garcia Blanco, R.M., 2004. Reevaluation of historic earthquakes in Spain, *Seismol. Res. Lett.,* **75**(17), 5–81.

Ni, J., 1978. Contemporary tectonics in the Tien Shan region, *Earth planet. Sci. Lett.,* **41,** 347–354.

Oth, A., Bindi, D., Parolai, S. & Wenzel, F., 2008. S-wave attenuation characteristics beneath the Vrancea region in Romania: new insights from the inversion of ground-motion spectra, *Bull. seism. Soc. Am.,* **98,** 2482–2497, doi:10.1785/0120080106.

Oth, A., Bindi, D., Parolai, S. & Di Giacomo, D., 2011. Spectral Analysis of K-NET and KiK-net Data in Japan, Part II: on Attenuation Characteristics, Source Spectra, and Site Response of Borehole and Surface Stations, *Bull. seism. Soc. Am.,* **101,** 667–687, doi:10.1785/0120100135.

Patriat, P. & Achache, J., 1984. The chronology of the India-Eurasia collision. Implications for crustal shortening and the driving mechanism of plates, *Nature,* **311,** 615–621.

Rautian, T.G., 1960. Energy of earthquakes, in *Methods for the Detailed Study of Seismicity,* pp. 75–114, ed. Riznichenko, Y.V., Izdatel'stvo Akademii Nauk SSSR, Moscow (in Russian).

Rautian, T., Khalturin, V., Fujita, K., Mackey, K.G. & Kendall, A.D., 2007. Origins and methodology of the russian energy k-class system and its relationship to magnitude scales, *Seismol. Res Lett.,* **78,** 579–590.

Szeliga, W., Hough, S., Martin, S. & Bilham, R., 2010. Intensity, magnitude, location and attenuation in India for felt earthquakes since 1762, *Bull. seism. Soc. Am.,* **100**(25), 70–584.

Toppozada, T.R., 1975. Earthquake magnitude as a function of intensity data in California and western Nevada, *Bull. seism. Soc. Am.,* **65,** 1223–1238.

Toppozada, T.R., Real, C.R. & Parke, D.L., 1981. Preparation of isoseismal maps and summaries of reported effects for pre-1900 California earthquakes, Calif. Div. Mines Geol. Open-File Rept, 81–11 SAC, 182.

Toppozada, T.R. & Branum, D.M., 2002. California M 1 5.5 earthquakes, history and areas damaged, in *International Handbook of Earthquake and Engineering Seismology,* eds Lee, W.H.K., Kanamori, H. & Jennings, P.C., International Association of Seismology and Physics of the Earth's Interior, Academic Press, San Diego.

Ulomov, V.I., 1999. The GSHAP Region 7 working group. Seismic hazard of Northern Eurasia, *Ann. Geofis.,* **4,** 1023–1038.

Zubovich, A.V. *et al.*, 2010. GPS velocity field for the Tien Shan and surrounding regions, *Tectonics,* **29**(TC6014), doi:10.1029/2010TC002772.

APPENDIX

Central Asia is a complex tectonic area that accommodates a large component of the continental collision between the Indian and Eurasian plates. To investigate the existence of possible regional dependency in the intensity attenuation characteristics, we first assess the spatial variability of intensity residuals computed with respect to the predictions obtained by applying regional attenuation models. To be consistent in the assumptions made in this study (e.g. assumed depth value, number of bootstrap replications, etc.), we derived an intensity prediction equation (IPE) using the data set analysed by Bindi *et al.* (2011) without considering the 1985 Xinjiang earthquake. It is composed of 70 earthquakes (Fig. A1) with locations and magnitudes taken from the CASRI catalogue. In particular, it also includes the calibration and validation earthquakes analysed in this study. The earthquakes are geographically grouped into three areas that can be considered to deform uniformly (Zubovich *et al.* 2010; Zubovich personal communication). These regions are sketched in Fig. A1, and correspond to the Pamir region, bounded to the north by the Alai valley and to the east by the Tarim basin (region R1, green circles), the Tien-Shan area located west of the Talas-Fergana fault and surrounding the Fergana basin (region R2, grey circles) and the Tien-Shan area located east of the Talas-Fergana fault and bounded to the south by the Tarim Basin (region R3, red circles). The numbers of earthquakes used are 10, 33 and 17 for region R1, R2, R3, respectively, whereas the number of intensity assignments for the same regions are 1025, 3083 and 1756, respectively.

The resulting residuals are shown in Fig. A2, using different colours for different regions. The estimations are unbiased for all regions, and showing similar standard deviations (0.63, 0.56 and 0.59 for regions R1, R2 and R3, respectively). This result suggests that the regional model represents on average the attenuation of intensities in the three considered regions equally well.

Finally, a set of IPEs is derived by analysing the earthquake in each region separately. The three models are shown in Fig. A3, where they are compared to the model derived considering all the data together. The models show a good agreement, with small differences only for distances greater than 200 km, where the attenuation for region R2 is weaker than for region R3. Considering that for these distances the regressions are strongly influenced by the applied constraints (e.g. degree of smoothness of the attenuation model), as a consequence of the few available data for the regressions when each region is treated separately from the others, these differences are not considered to be significant.

In conclusion, this analysis performed over the available intensity data does not support the introduction of subregional models. Although the closeness of the intensity attenuation models obtained for the three regions need not imply that later variations in the attenuation characteristics do not exist in such a complex tectonic setting, such differences are probably masked by the nature of the intensity data.

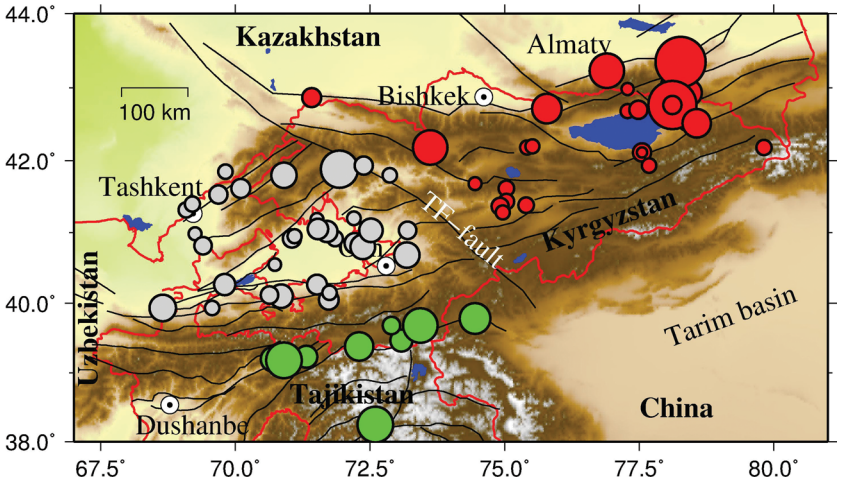

Figure A1. Earthquakes (circles) used to investigate the existence of regional attenuation properties. The three different colours identify regions R1 (green), R2 (grey) and R3 (red) (see Appendix).

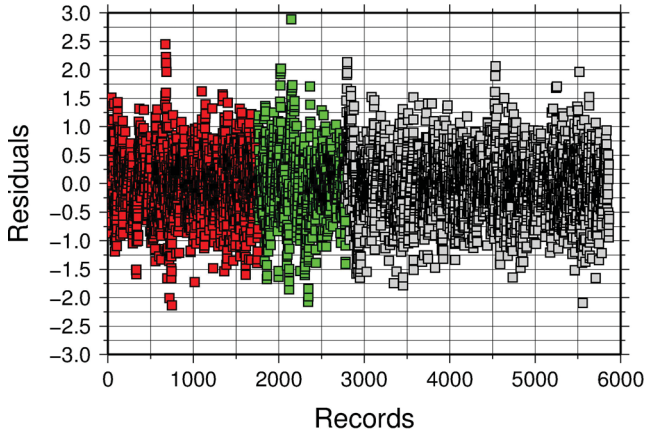

Figure A2. Residuals from the model for the entire area coloured accordingly to regions R1, R2, R3 as shown in Fig. A1.

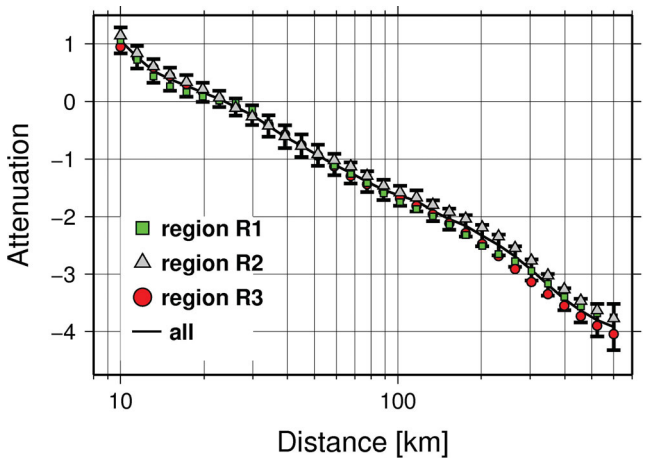

Figure A3. Non-parametric attenuation models derived for regions R1 (green), R2 (grey) and R3 (red) as shown in Fig. A1. The non-parametric model calibrated while considering all the data is shown as the black line (median) and vertical bar (95 per cent confidence interval from bootstrap analysis).